

An experimental test of all theories with predictive power beyond quantum theory

Terence E. Stuart,^{1,*} Joshua A. Slater,^{1,†} Roger Colbeck,^{2,‡} Renato Renner,^{3,§} and Wolfgang Tittel^{1,¶}

¹*Institute for Quantum Information Science, and Department of Physics and Astronomy,
University of Calgary, 2500 University Drive NW, Calgary, Alberta T2N 1N4, Canada.*

²*Perimeter Institute for Theoretical Physics, 31 Caroline Street North, Waterloo, Ontario N2L 2Y5, Canada.*

³*Institute for Theoretical Physics, ETH Zurich, 8093 Zurich, Switzerland.*

According to quantum theory, the outcomes of future measurements cannot (in general) be predicted with certainty. In some cases, even with a complete physical description of the system to be measured and the measurement apparatus, the outcomes of certain measurements are completely random. This raises the question, originating in the paper by Einstein, Podolsky and Rosen [1], of whether quantum mechanics is the optimal way to predict measurement outcomes. Established arguments and experimental tests exclude a few specific alternative models [2–15]. Here, we provide a complete answer to the above question, refuting any alternative theory with significantly more predictive power than quantum theory. More precisely, we perform various measurements on distant entangled photons, and, under the assumption that these measurements are chosen freely, we give an upper bound on how well any alternative theory could predict their outcomes [16]. In particular, in the case where quantum mechanics predicts two equally likely outcomes, our results are incompatible with any theory in which the probability of a prediction is increased by more than ~ 0.19 . Hence, we can immediately refute any already considered or yet-to-be-proposed alternative model with more predictive power than this.

Many of the predictions we make in everyday life are probabilistic. Usually this is caused by having incomplete information, as is the case when making weather forecasts. On the other hand, even with all the information available within quantum mechanics, the outcome of certain experiments, e.g., the path taken by a spin-half particle in a Stern-Gerlach experiment, is generally not predictable before the start of the experiment. This lack of predictive power has prompted a long debate, which in turn led to important fundamental insights. In particular, Kochen and Specker, and independently Bell, proved that there cannot exist any *noncontextual* theory that predicts observations with certainty [17, 18]. In a similar vein, Bell showed [2] that in general there cannot exist any additional hidden property of the particle (a *local hidden variable*) that completely determines the outcome of any measurement on the particle (for an illustration of such a model see Fig. 1). Bell’s argument relies on the fact that entangled particles give rise to correlations that cannot be reproduced in any local hidden variable theory. The existence of such correlations has been confirmed in a series of increasingly sophisticated experiments [5–9, 11].

The purpose of the above arguments was to refute theories in which hidden parameters determine any experimental outcomes. Access to these parameters would allow us, in principle, to predict the outcomes of any experiment with certainty. However, these arguments do not preclude the possibility that we find a theory that has more predictive power than quantum mechanics, while remaining probabilistic. Consider again the Stern-Gerlach example where, according to quantum mechanics, a particle entering the apparatus with a certain spin orientation may be deviated in one of two directions, each with probability 0.5. One may now conceive of a theory that, depending on an additional parame-

ter, would allow us to predict the direction of deviation with a larger probability, say 0.75, thereby improving the quantum mechanical prediction by 0.25. In Fig. 1 we describe an example of such a theory, which essentially corresponds to a proposal put forward by Leggett [4].

In this Letter we present experimental data that bounds the probability, δ , by which any alternative theory could improve upon predictions made by quantum theory while still being consistent with the assumption that measurement settings can be chosen freely. We find that quantum theory is close to optimal in terms of its predictive power. Our work relies on a recent theoretical argument [16], which is itself based on a sequence of work [19–23], partly in the area of quantum cryptography. The experiment requires measuring bipartite correlations of entangled particles, as well as establishing the distributions of the associated individual measurement outcomes, for a sufficiently large number of measurement settings. The maximum increase of predictive power, δ , of any alternative theory then depends on the strength of the measured correlations, I , and on the bias in the individual outcomes, ν :

$$\delta \leq \frac{I}{2} + \nu. \quad (1)$$

(These quantities are defined in the Appendix, where we also explain the procedure for obtaining I and ν from experimental data.)

Before describing the experimental setup, let us briefly review the main features of the theory leading to Eq. 1 (a complete derivation is given in the Appendix). Crucially, the framework used is operational, in the sense that it refers only to directly observable quantities, such as measurement outcomes. For example, the Stern-Gerlach experiment mentioned above outputs a binary value, X ,

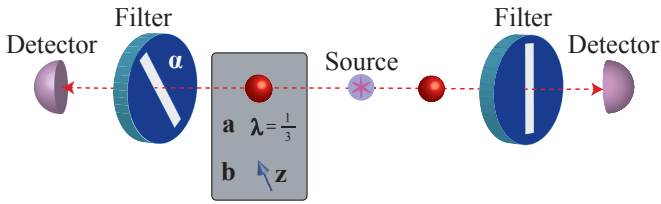


FIG. 1: **Two alternative models.** Consider an experiment in which a source emits two spin-half particles travelling to two distant sites. Their spin direction is measured, e.g., by letting them pass through a filter that absorbs particles with the opposite spin direction. If the particles are initially maximally entangled, then the probability of correctly predicting whether the particle on the left is transmitted by the filter, which has a direction α , is, according to quantum mechanics, given by $p_{\text{QM}} = 0.5$. **a**, Bell’s model of hidden variables [18] as an example for an alternative deterministic theory. Bell proposed a model in which the outcome of such a measurement is precisely determined by the particle’s quantum mechanical state vector $|\psi\rangle$, the measurement specified by α , and an additional real number λ – a local hidden variable (LHV) that is not present in standard quantum mechanics. If we had access to λ , we could predict the outcome of the measurement with certainty, hence $p_{\text{LHV}} = 1$. **b**, A Leggett-type model [4] as an example for an alternative probabilistic theory. Leggett imagined a theory in which each particle carries a hidden parameter, specified as a vector \mathbf{z} that may be seen as a “classical spin”. His model, adapted to general spin particles, prescribes that the probability that a particle with vector \mathbf{z} is transmitted by a filter in direction α is given by $\frac{1}{2} + \mathbf{z} \cdot \alpha$. Since the vector \mathbf{z} is unknown, we model it here as a random variable with no preferred direction (a detailed discussion of this and other distributions over \mathbf{z} is deferred to the Appendix). A straightforward calculation then shows that, if we had access to the parameter \mathbf{z} , we could on average correctly predict the outcome with probability $p_{\text{Leggett}} = 0.75$.

indicating in which direction the particle deviated. We associate with X a time coordinate t and three spatial coordinates (x_1, x_2, x_3) , corresponding to a point in spacetime where the value X can be observed. (If the value can be observed at different points in space time, we may define further copies of X with different spacetime coordinates.) We note that these coordinates can be determined operationally (e.g., using clocks and measuring rods, with respect to a fixed reference system). We call such observable values with spacetime coordinates *space-time variables (SVs)*. In the same manner, any parameter that is needed to specify the experiment (e.g., the orientation of the Stern-Gerlach apparatus) can be modelled as an SV.

Consider now an experiment in which a spin measurement is made on a particle that is maximally entangled with another one. According to quantum theory, the outcome, X , of this measurement is random, even with a complete description of the measurement apparatus, A . However, an alternative theory may provide us with additional information, Ξ (which can also be modelled in

terms of SVs [16]). We can then ask whether this additional information Ξ can be used to improve the predictions that quantum mechanics makes about X , which depend on the measurement setting A and the initial state (which we assume to be fixed). This question has a negative answer if the distribution of X , conditioned on A , is unchanged when we learn Ξ . This can be expressed in terms of the Markov chain condition [25],

$$X \leftrightarrow A \leftrightarrow \Xi$$

Equation 1 now places a bound on the maximum probability, δ , by which this condition is violated. In other words, the predictions obtained from quantum theory are optimal except with probability (at most) δ .

For the specific measurement described above, the validity of Eq. 1 relies only on the natural (and often implicit) assumption that measurement parameters can be chosen freely. This assumption can be expressed in the above framework as the requirement that the SV corresponding to a measurement parameter, A , can be chosen such that it is statistically independent of all SVs whose coordinates lie outside the future lightcone of A (Bell’s theorem also relies on such an assumption, for example, as explained in Ref. 26). When interpreted within the usual relativistic spacetime structure, this is equivalent to demanding that A is uncorrelated with any pre-existing values in any frame. We also note that this requirement can be seen as a prerequisite for non-contextuality, as pointed out in Ref. 24 (where an alternative proof that quantum theory cannot be extended, based on the assumption of non-contextuality, is offered).

We note that our bound on the predictive power of alternative theories can be extended to arbitrary measurements (not necessarily on maximally entangled particles) if one makes one additional assumption. This assumption is that the evolution of the state of a physical system can always be correctly described by a unitary operation if one includes part of the environment in the description of the process [16].

The experimental setup we use to bound the quantities on the right-hand side of Eq. 1 is detailed in Fig. 2. Our source [27] generates photon pairs with high fidelity to the entangled state

$$|\phi^+\rangle = \frac{1}{\sqrt{2}}(|HH\rangle + |VV\rangle), \quad (2)$$

where $|H\rangle$ and $|V\rangle$ represent horizontal and vertical polarization states, respectively, and replace the usual spin-up and spin-down notation for spin-half particles. The photons from each pair are separated and sent towards polarization analyzers that can be adjusted to measure the polarization of an incoming photon along any desired direction $\mathbf{S} = (S_+, S_L, S_H)$, where the three-component vector \mathbf{S} is expressed in terms of its projections onto diagonal ($+45^\circ$), left-circular (L), and horizontal (H) po-

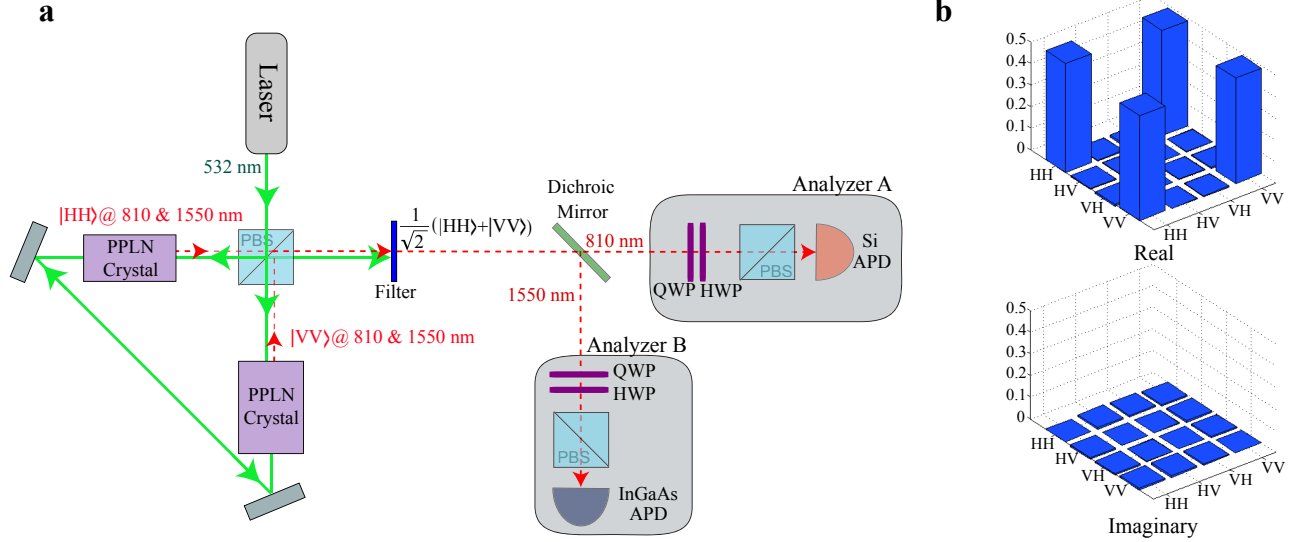


FIG. 2: **Generating and measuring entangled states.** **a**, Experimental setup. A diagonally polarized, continuous wave, 532 nm wavelength laser beam is split by a polarizing beam splitter (PBS) and travels both clockwise and counter-clockwise through a polarization Sagnac interferometer. The interferometer contains two type-I, periodically poled lithium niobate (PPLN) crystals configured to produce collinear, non-degenerate, 810/1550 nm wavelength photon pairs by means of spontaneous parametric down-conversion. As photon-pair generation is polarization dependent, the clockwise-travelling, vertically polarized (counter-clockwise travelling, horizontally polarized) pump light passes through the first crystal without interaction and may down-convert in the second crystal to produce two horizontally (vertically) polarized photons. For sufficiently small pump power, recombination of the two bi-photon modes on the PBS yields the entangled $|\phi^+\rangle$ state. After exiting the interferometer, the remaining pump light is filtered out using a high-pass filter. The entangled photons are separated on a dichroic mirror and sent to analyzers that allow one to measure polarization along any desired direction on the Bloch sphere. They consist of quarter wave plates (QWP), half wave plates (HWP), PBSs and single photon detectors. The 810 nm photons are detected using a free-running Silicon avalanche photo-diode (Si APD), and 1550 nm photons are detected using an InGaAs APD triggered by detection events from the Si APD. **b**, Density matrix. Density matrix ρ_{real} of the bi-photon state produced by our source as calculated via maximum-likelihood quantum state tomography [28] (see the Appendix for actual values). The fidelity, $F = \langle \phi^+ | \rho_{\text{real}} | \phi^+ \rangle$, between the detected state, ρ_{real} , and the ideal state, $|\phi^+\rangle$, given by Eq. 2, is $(98.1 \pm 0.1)\%$.

larized components. \mathcal{S} is conveniently depicted on the Bloch sphere, see Fig 3.

We perform a series of experiments that are parameterized by an integer, N . Each experiment yields a value, $\delta_N = I_N/2 + \nu_N$, and we bound δ by the minimum over all measured δ_N . Each experiment comprises N pairs of opposing spin measurement settings per analyzer (i.e., N different bases):

$$\mathcal{S}_A(m) = \begin{pmatrix} \cos\left(m\frac{\pi}{2N}\right) \\ \sin\left(m\frac{\pi}{2N}\right) \\ 0 \end{pmatrix}, m \in \{0, 2, 4, \dots, (4N-2)\}, \quad (3)$$

and

$$\mathcal{S}_B(n) = \begin{pmatrix} \cos\left(n\frac{\pi}{2N}\right) \\ -\sin\left(n\frac{\pi}{2N}\right) \\ 0 \end{pmatrix}, n \in \{1, 3, 5, \dots, (4N-1)\}. \quad (4)$$

For each setting $\mathcal{S}_A(m)$, we count detected photons over 80 sec to establish the bias ν_N . Furthermore, for certain joint measurements (described by specific combinations

N	I_N	ν_N	δ_N
2	0.6196 ± 0.0049	0.0027 ± 0.0003	0.3125 ± 0.0025
3	0.4802 ± 0.0046	0.0036 ± 0.0003	0.2437 ± 0.0023
4	0.4103 ± 0.0046	0.0043 ± 0.0003	0.2094 ± 0.0023
5	0.3940 ± 0.0045	0.0045 ± 0.0003	0.2015 ± 0.0023
6	0.3791 ± 0.0041	0.0047 ± 0.0003	0.1942 ± 0.0021
7	0.3872 ± 0.0042	0.0048 ± 0.0003	0.1984 ± 0.0021

TABLE I: **Summary of Results.** The table shows values for I_N , bias ν_N , as well as $\delta_N = I_N/2 + \nu_N$. Statistical uncertainties (one standard deviation) are calculated from measurement results assuming Poissonian statistics.

of $\mathcal{S}_A(m)$ and $\mathcal{S}_B(n)$, we also register the number of detected photon pairs over 40 sec to calculate I_N , and hence δ_N (see the Appendix).

Our experimental results are depicted in Fig. 3 and summarized in Table I. We measured δ_N for $N = 2$ to $N = 7$ and found the minimum, $\delta_6 = 0.194 \pm 0.003$, for $N = 6$. Hence, the probability by which the pre-

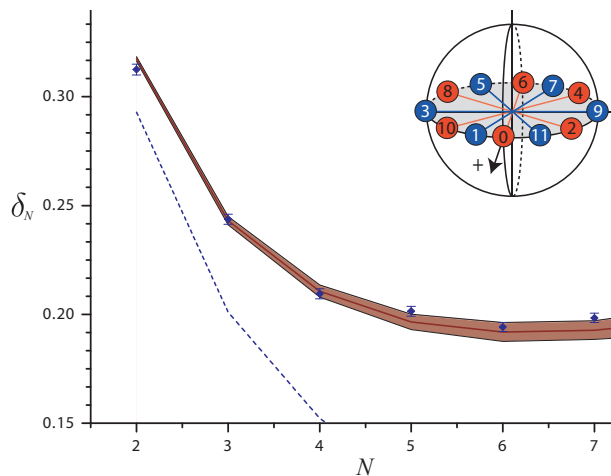


FIG. 3: **Measurements and results.** **a**, Measurement settings. Graphical depiction of the polarization measurements along \mathcal{S}_A (red) and \mathcal{S}_B (blue). The example shows $N = 4$. **b**, Results. Experimentally obtained values δ_N (blue diamonds) with one-standard-deviation uncertainties calculated from measurement results assuming Poissonian statistics. Also shown is a curve joining the values predicted by quantum theory, including one-standard-deviation statistical uncertainties (solid red line and grey shaded area, respectively), calculated from the measured density matrix ρ_{real} . The bounds of the shaded region are derived using Monte Carlo simulations and are consistent with the observed variations of the measured values. Finally, the dashed blue line is the theoretical curve, again calculated using quantum theory, that assumes the ideal $|\phi^+\rangle$ state, as in Eq. 2, and perfect experimental apparatus with zero noise. It asymptotically approaches zero as N tends to infinity. For instance, for $N = 6$ we find $\delta_6^{\text{ideal}} = 0.102$.

dictions made by quantum theory can be improved using any alternative theory is at most ~ 0.19 . As examples, note that this value rules out local hidden variable as well as Leggett-type models (as explained in Fig. 1 and the Appendix), since $p_{\text{LHV}} - p_{\text{QM}} = 0.5 > \delta$ and $p_{\text{Leggett}} - p_{\text{QM}} = 0.25 > \delta$, respectively. (Here, p denotes the maximum probability of correctly predicting the measurement outcome in the model/theory indicated in the subscript.) We remark that our experiments do not close the locality and detection loopholes, so, strictly, the above conclusions hold modulo the assumption that similar experiments closing these loopholes would show the same results.

In conclusion, under the assumption that measurements can be chosen freely, no theory can predict measurement outcomes substantially better than quantum mechanics. In other words, any already considered or yet-to-be-proposed theory that makes significantly better predictions would either be incompatible with the experimental observations presented herein, or be incom-

patible with our assumption that the measurement parameters can be chosen freely. While the former is true, for example, for local hidden variable theories (as already pointed out by Bell [2]) or for the Leggett model [4], the de Broglie-Bohm theory [29, 30] is an example of the second type—the theory cannot incorporate measurement parameters that satisfy our free choice assumption.

ACKNOWLEDGEMENTS

The authors thank F. Bussi eres for help with setting up the photon pair source, and V. Kiselyov for technical support. Research at Perimeter Institute is supported by the Government of Canada through Industry Canada and by the Province of Ontario through the Ministry of Research and Innovation. R.R. acknowledges support from the Swiss National Science Foundation (grant No. 200020-135048 and the NCCR QSIT) and from the European Research Council (grant No. 258932). W.T., T.E.S. and J.A.S. are supported by NSERC, QuantumWorks, General Dynamics Canada, iCORE (now part of Alberta Innovates), CFI, and AAET.

* testuart@ucalgary.ca
† jslater@qis.ucalgary.ca
‡ rcolbeck@perimeterinstitute.ca
§ renner@phys.ethz.ch
¶ wtittel@ucalgary.ca

- [1] Einstein, A., Podolsky, B. & Rosen, N. Can quantum-mechanical description of physical reality be considered complete? *Physical Review* **47**, 777–780 (1935).
- [2] Bell, J. S. On the Einstein-Podolsky-Rosen paradox. In *Speakable and unspeakable in quantum mechanics*, chap. 2 (Cambridge University Press, 1987).
- [3] Greenberger, D. M., Horne, M. & Zeilinger, A. Going beyond Bell’s theorem. *Bell’s Theorem, Quantum Theory, and Conceptions of the Universe* (Kluwer Academic, Dordrecht, The Netherlands., 1989), 69–72. M. Kafatos, editor.
- [4] Leggett, A. J. Nonlocal hidden-variable theories and quantum mechanics: An incompatibility theorem. *Foundations of Physics* **33**, 1469–1493 (2003).
- [5] Freedman, S. J. & Clauser, J. F. Experimental test of local hidden-variable theories. *Physical Review Letters* **28**, 938–941 (1972).
- [6] Aspect, A., Grangier, P. & Roger, G. Experimental realization of Einstein-Rosen-Bohm gedankenexperiment: A new violation of Bell’s inequalities. *Physical Review Letters* **49**, 91–94 (1982).
- [7] Tittel, W. *et al.* Experimental demonstration of quantum correlations over more than 10 km. *Physical Review A* **57**, 3229–3232 (1998).
- [8] Weihs, G., Jennewein, T., Simon, C., Weinfurter, H. & Zeilinger, A. Violation of Bell’s inequality under strict Einstein locality conditions. *Physical Review Letters* **81**, 5039–5043 (1998).

- [9] Rowe, M. A., Kielpinski, D., Meyer, V., Sackett, C. A., Itano, W. M., Monroe, C. & Wineland, D. J. Experimental violation of a Bell's inequality with efficient detection. *Nature* **409**, 791–794 (2001).
- [10] Aspect, A. Bell's inequality test: More ideal than ever. *Nature* **398**, 189–190 (1999).
- [11] Pan, J.-W., Bouwmeester, D., Daniell, M., Weinfurter H. & Zeilinger, A. Experimental test of quantum non-locality in three-photon Greenberger-Horne-Zeilinger entanglement. *Nature* **403**, 515–519 (2000).
- [12] Gröblacher, S. *et al.* An experimental test of non-local realism. *Nature* **446**, 871–875 (2007).
- [13] Branciard, C. *et al.* Experimental falsification of Leggett's non-local variable model. *Physical Review Letters* **99**, 210407 (2007).
- [14] Eisaman, M. D., Goldschmidt, E. A., Chen, J., Fan, J. & Migdall, A. Experimental test of nonlocal realism using a fiber-based source of polarization-entangled photon pairs. *Phys. Rev. A* **77**, 032339 (2008).
- [15] Branciard, C. *et al.* Testing quantum correlations versus single-particle properties within Leggett's model and beyond. *Nature Physics* **4**, 681–685 (2008).
- [16] Colbeck, R. & Renner, R. Quantum theory cannot be extended. e-print [arXiv:1005.5173](https://arxiv.org/abs/1005.5173) (2010).
- [17] Kochen, S. & Specker, E. P. The problem of hidden variables in quantum mechanics. *Journal of Mathematics and Mechanics* **17**, 59–87 (1967).
- [18] Bell, J. S. On the problem of hidden variables in quantum mechanics. In *Speakable and unspeakable in quantum mechanics*, chap. 1 (Cambridge University Press, 1987).
- [19] Pearle, P. M. Hidden-variable example based upon data rejection. *Physical Review D* **2**, 1418–1425 (1970).
- [20] Braunstein, S. L. & Caves, C. M. Wringing out better Bell inequalities. *Annals of Physics* **202**, 22–56 (1990).
- [21] Barrett, J., Hardy, L. & Kent, A. No signalling and quantum key distribution. *Physical Review Letters* **95**, 010503 (2005).
- [22] Barrett, J., Kent, A. & Pironio, S. Maximally non-local and monogamous quantum correlations. *Physical Review Letters* **97**, 170409 (2006).
- [23] Colbeck, R. & Renner, R. Hidden variable models for quantum theory cannot have any local part. *Physical Review Letters* **101**, 050403 (2008).
- [24] Chen, Z. & Montina, A. Measurement contextuality is implied by macroscopic realism. e-print [arXiv:1012.2122](https://arxiv.org/abs/1012.2122) (2010).
- [25] Cover, T. M. & Thomas, J. A. *Elements of Information Theory* (John Wiley and Sons Inc., 2006), 2nd edn. Section 2.8.
- [26] Bell, J. S. Free variables and local causality. In *Speakable and unspeakable in quantum mechanics*, chap. 12 (Cambridge University Press, 1987).
- [27] Stuart, T. E., Slater, J. A., Bussières, F., & Tittel, W. In preparation. (2011).
- [28] Altepeter, J. B., Jeffrey, E. R. & Kwiat, P. G. Photonic state tomography. *Advanced Atomic and Optical Physics* **52**, 105–159 (2005).
- [29] de Broglie, L. La mécanique ondulatoire et la structure atomique de la matière et du rayonnement. *Journal de Physique, Serie VI* **VIII**, 225–241 (1927).
- [30] Bohm, D. A suggested interpretation of the quantum theory in terms of "hidden" variables. I. *Physical Review* **85**, 166–179 (1952).
- [31] Suarez, A. Why aren't quantum correlations maximally nonlocal? Biased local randomness as essential feature of quantum mechanics. e-print [arXiv:0902.2451](https://arxiv.org/abs/0902.2451) (2009).

APPENDIX

Calculation of bias, ν_N , and correlation strength, I_N

The bias is a measure of how close the distribution of the individual measurement outcomes, X , is to uniform. It is calculated from the number of 810 nm wavelength photons detected in opposing spin measurements. In general, this number is not the same for all pairs of measurements. We take the bias, ν_N , to be the maximum over the individual biases. Denoting the number of detected photons for setting $\mathcal{S}_A(m)$ by $M(m)$, we have:

$$\nu_N = \frac{1}{2} \max_{a \in \{0, 2, 4, \dots, (2N-2)\}} \left\{ \frac{|M(a) - M(a + 2N)|}{M(a) + M(a + 2N)} \right\}. \quad (5)$$

The quantity I_N measures the strength of the bipartite correlation between two analyzers. It is defined by

$$I_N = P(0, 2N - 1) + \sum_{\substack{a, b \\ |a-b|=1}} (1 - P(a, b)) \quad (6)$$

where $a \in \{0, 2, 4, \dots, (2N - 2)\}$, $b \in \{1, 3, 5, \dots, (2N - 1)\}$. Furthermore, $P(a, b)$ is the sum of the probabilities for detecting two photons from a pair along the spin vectors $\mathcal{S}_A(a)$ and $\mathcal{S}_B(b)$, and along $-\mathcal{S}_A(a)$ and $-\mathcal{S}_B(b)$ (i.e. the probability of correlated outcomes):

$$P(a, b) = \frac{M(a, b) + M(a + 2N, b + 2N)}{M(a, b) + M(a, b + 2N) + M(a + 2N, b) + M(a + 2N, b + 2N)} \quad (7)$$

where, e.g., $M(a, b)$ is the number of joint photon detections for measurements along $\mathcal{S}_A(a)$ and $\mathcal{S}_B(b)$.

Proof of the bound

In this section, we prove the bound given in Equation (1) in the main text, which is stated as Lemma 1 below. We use a bipartite scenario in which two spacelike separated measurements are performed on a maximally entangled state. We denote the choices of observable $A \in \{0, 2, \dots, 2N - 2\}$ and $B \in \{1, 3, \dots, 2N - 1\}$ and their outcomes $X \in \{+1, -1\}$ and $Y \in \{+1, -1\}$, respectively¹. We additionally consider information that might be provided by an alternative theory (this was denoted Ξ in the main text), which is modelled as an additional system with input C and output Z [16]. If one makes the assumption that the measurements can be chosen freely, then the joint distribution $P_{XYZ|ABC}$ satisfies the non-signaling conditions

$$P_{XY|ABC} = P_{XY|AB} \quad (8)$$

$$P_{XZ|ABC} = P_{XZ|AC} \quad (9)$$

$$P_{YZ|ABC} = P_{YZ|BC} \quad (10)$$

(see [16] for a short proof of this).

Lemma 1 gives a bound on the increase in predictive power of any alternative theory in terms of the strength of correlations and the bias of the individual outcomes. The bound is expressed in terms of the variational distance $D(P_Z, Q_Z) := \frac{1}{2} \sum_z |P_Z(z) - Q_Z(z)|$, which has the following operational interpretation: if two distributions have variational distance at most δ , then the probability that we ever notice a difference between them is at most δ .

The bias is quantified by² $\nu_N := \max_a D(P_{X|a}, P_{\bar{X}})$, where $P_{\bar{X}}$ is the uniform distribution on X . To quantify the correlation strength, we define

$$I_N := P(X = Y | A = 0, B = 2N - 1) + \sum_{\substack{a, b \\ |a-b|=1}} P(X \neq Y | A = a, B = b). \quad (11)$$

¹ Note that the measurements we speak of in the Appendix have a slightly different form than those in the main text. Specifically, we now assume that measurements behave ideally, projecting onto one of two basis elements and leading to one of the two outcomes ± 1 . In a real experiment, there is always the additional possibility of no photon detection (let us denote this outcome 0). The measurements discussed in the main text are configured to distinguish $+1$ from either -1 or 0, or to distinguish -1 from either $+1$ or 0. Both measurements are used in the experiment to infer the distribution of the ideal measurement with outcomes ± 1 .

² A note on notation: we usually use lower case to denote particular instances of upper case random variables.

This is equivalent to Equation (6) in the main text. We remark that $I_N \geq 1$ is a Bell inequality, i.e. is satisfied by any local hidden variable model.

Lemma 1. *For any non-signalling probability distribution, $P_{XYZ|ABC}$, we have*

$$D(P_{Z|abcx}, P_{Z|abc}) \leq \delta_N := \frac{I_N}{2} + \nu_N \quad (12)$$

for all a, b, c , and x .

To connect this back to the main text, we remark that the Markov chain condition $X \leftrightarrow A \leftrightarrow \Xi$ is equivalent to $P_{Z|abcx} = P_{Z|abc}$ (which corresponds to Ξ not being of use to predict X). Hence, from the operational meaning of the variational distance (given above), the left-hand-side of (12) corresponds to the maximum increase in the probability of correctly predicting the outcome X , denoted δ in the main text.

The proof is an extension of an argument given in [16] which is based on *chained Bell inequalities* [19, 20] and generalizes results of [21–23]. Many steps of this proof mirror those in [16], which we repeat for completeness. Furthermore, note that the bound derived in this Lemma is tighter than that of [16].

Proof. We first consider the quantity I_N evaluated for the conditional distribution $P_{XY|AB,cz} = P_{XY|ABCZ}(\cdot, \cdot | \cdot, \cdot, c, z)$, for any fixed c and z . The idea is to use this quantity to bound the variational distance between the conditional distribution $P_{X|acz}$ and its negation, $1 - P_{X|acz}$, which corresponds to the distribution of X if its values are interchanged. If this distance is small, it follows that the distribution $P_{X|acz}$ is roughly uniform.

For $a_0 := 0, b_0 := 2N - 1$, we have

$$\begin{aligned} I_N(P_{XY|AB,cz}) &= P(X = Y | A = a_0, B = b_0, C = c, Z = z) + \sum_{\substack{a,b \\ |a-b|=1}} P(X \neq Y | A = a, B = b, C = c, Z = z) \\ &\geq D(1 - P_{X|a_0b_0cz}, P_{Y|a_0b_0cz}) + \sum_{\substack{a,b \\ |a-b|=1}} D(P_{X|abcz}, P_{Y|abcz}) \\ &= D(1 - P_{X|a_0cz}, P_{Y|b_0cz}) + \sum_{\substack{a,b \\ |a-b|=1}} D(P_{X|acz}, P_{Y|bcz}) \\ &\geq D(1 - P_{X|a_0cz}, P_{X|a_0cz}) \\ &= 2D(P_{X|a_0b_0cz}, P_{\bar{X}}). \end{aligned} \quad (13)$$

The first inequality follows from the fact that $D(P_{X|\Omega}, P_{Y|\Omega}) \leq P(X \neq Y | \Omega)$ for any event Ω (a short proof of this can be found in [23]). Furthermore, we have used the non-signalling conditions $P_{X|abcz} = P_{X|acz}$ (from (9)) and $P_{Y|abcz} = P_{Y|bcz}$ (from (10)), and the triangle inequality for D . By symmetry, this relation holds for all a and b . We hence obtain $D(P_{X|abcz}, P_{\bar{X}}) \leq \frac{1}{2} I_N(P_{XY|AB,cz})$ for all a, b, c and z .

We now take the average over z on both sides of (13). First, the left hand side gives

$$\begin{aligned} \sum_z P_{Z|abc}(z) I_N(P_{XY|AB,cz}) &= \sum_z P_{Z|c}(z) I_N(P_{XY|AB,cz}) \\ &= \sum_z P_{Z|a_0b_0c}(z) P(X = Y | a_0, b_0, c, z) + \sum_{\substack{a,b \\ |a-b|=1}} \sum_z P_{Z|abc}(z) P(X \neq Y | a, b, c, z) \\ &= P(X = Y | a_0, b_0, c) + \sum_{\substack{a,b \\ |a-b|=1}} P(X \neq Y | a, b, c) \\ &= I_N(P_{XY|AB,c}), \end{aligned} \quad (14)$$

where we used the non-signalling condition $P_{Z|abc} = P_{Z|c}$ (which is implied by (9) and (10)) several times. Next, taking the average on the right hand side of (13) yields $\sum_z P_{Z|abc}(z) D(P_{X|abcz}, P_{\bar{X}}) = D(P_{XZ|abc}, P_{\bar{X}} \times P_{Z|abc})$, so we have

$$2D(P_{XZ|abc}, P_{\bar{X}} \times P_{Z|abc}) \leq I_N(P_{XY|AB,c}) = I_N(P_{XY|AB}). \quad (15)$$

The last equality follows from the non-signalling condition (8) (if $P(X = Y | a, b, c)$ or $P(X \neq Y | a, b, c)$ depended on c , then there would be signalling from C to A and B).

Furthermore, note that

$$2D(P_{XZ|abc}, P_{\bar{X}} \times P_{Z|abc}) = \sum_z |P_{XZ|abc}(-1, z) - \frac{1}{2}P_{Z|abc}(z)| + \sum_z |P_{XZ|abc}(+1, z) - \frac{1}{2}P_{Z|abc}(z)|$$

and that both of the terms on the right hand side are equal (since $P_{Z|abc}(z) = P_{XZ|abc}(-1, z) + P_{XZ|abc}(+1, z)$) i.e. $\sum_z |P_{XZ|abc}(x, z) - \frac{1}{2}P_{Z|abc}(z)| \leq \frac{I_N}{2}$ for all a, b, c and x . Note also that $D(P_{X|a}, P_{\bar{X}}) = |P_{X|a}(x) - \frac{1}{2}|$ for all x . Combining the above, we have

$$\begin{aligned} D(P_{Z|abcx}, P_{Z|abc}) &= \sum_z \left| \frac{1}{2}P_{Z|abcx}(z) - \frac{1}{2}P_{Z|abc}(z) \right| \\ &\leq \sum_z \left| \frac{1}{2}P_{Z|abcx}(z) - P_{X|abc}(x)P_{Z|abcx}(z) \right| + \sum_z \left| P_{X|abc}(x)P_{Z|abcx}(z) - \frac{1}{2}P_{Z|abc}(z) \right| \\ &= \sum_z P_{Z|abcx}(z) \left| \frac{1}{2} - P_{X|abc}(x) \right| + \sum_z \left| P_{XZ|abc}(x, z) - \frac{1}{2}P_{Z|abc}(z) \right| \\ &\leq D(P_{X|a}, P_{\bar{X}}) + \frac{I_N(P_{XY|AB})}{2}. \end{aligned}$$

This establishes the relation (12). □

Tightness

We can also establish that this bound is tight, as follows. Consider a classical model in which, with probability ε , we have $X = Y = Z = -1$, and otherwise $X = Y = Z = +1$ (independently of A, B and C). This distribution has $I_N(P_{XY|AB}) = 1$ and $\nu = \frac{1}{2} - \varepsilon$. It also satisfies $D(P_{Z|abcX=-1}, P_{Z|abc}) = 1 - \varepsilon$, which is equal to the bound implied by (12).

Application to Leggett models

In the Leggett model [4], one imagines that improved predictions about the outcomes for measurements on qubits are available. More precisely, each particle has an associated vector (thought of as a hidden direction of its spin) and the outcome distribution is expressed via the inner product with the vector describing the measurement (see Figure 1 in the main text). Denoting the hidden vector for the first particle by \mathbf{z} , and its measurement vector $\boldsymbol{\alpha}$ (this is the Bloch vector associated with the chosen measurement direction), its outcomes are distributed according to

$$P_{X|\boldsymbol{\alpha}\mathbf{z}}(\pm 1) = \frac{1}{2}(1 \pm \boldsymbol{\alpha} \cdot \mathbf{z}). \quad (16)$$

To relate this back to the discussion above, the Leggett model corresponds to the case that there is no C , and where the hidden vectors are contained in Z . Note that Leggett already showed his model to be incompatible with quantum theory [4] and experiments have since falsified it using specific inequalities [12, 13, 15]. Here we discuss the model in light of our experiment, which, it turns out, is sufficient to falsify it.

Note that, as presented in [4] and above, the model is not fully specified, since the distribution of the hidden vectors, \mathbf{z} , is not given. In order to discuss the implications of our experimental results, we refer to four cases (corresponding to different distributions over \mathbf{z}). Before describing these cases, we first note that (12) implies

$$\langle D(P_{X|\boldsymbol{\alpha}\mathbf{z}}, P_{\bar{X}}) \rangle_{\mathbf{z}} \leq \delta_N, \quad (17)$$

for all $\boldsymbol{\alpha}$, where $\langle \cdot \rangle_{\mathbf{z}}$ denotes the expectation value over the vectors \mathbf{z} . In order to falsify a particular version of the Leggett model, we compute δ_N^{crit} , the smallest increase in predictive power under the assumption that a particular version of the Leggett model is correct (i.e. the smallest value of the left-hand-side of (17) over all $\boldsymbol{\alpha}$). We then show that δ_N^{crit} is above the maximum increase in predictive power compatible with the experimental data, δ_N , hence falsifying that version of Leggett's model.

First Case: We imagine that the vector \mathbf{z} is a fixed vector (i.e. $P_{\mathbf{z}}(\mathbf{z}) = 1$) in the same plane on the Bloch sphere as our measurements. From (17) we find $D(P_{X|\boldsymbol{\alpha}\mathbf{z}}, P_{\bar{X}}) \leq \delta_N$ for all $\boldsymbol{\alpha}$. However, (16) implies $D(P_{X|\boldsymbol{\alpha}\mathbf{z}}, P_{\bar{X}}) = \frac{|\boldsymbol{\alpha} \cdot \mathbf{z}|}{2}$.

N	δ_N^{crit1}	δ_N^{crit2}	δ_N^{crit3}	δ_N^{crit4}	δ_N^1	δ_N^2
2	0.3536	0.2	0.25	0.1768	0.3125 ± 0.0025	
3	0.4330	0.3062	0.25	0.2165	0.2437 ± 0.0023	
4	0.4619	0.3266	0.25	0.2310	0.2094 ± 0.0023	
5	0.4755	0.3362	0.25	0.2378	0.2015 ± 0.0023	
6	0.4830	0.3415	0.25	0.2415	0.1942 ± 0.0021	0.2297 ± 0.0020
7	0.4875	0.3447	0.25	0.2437	0.1948 ± 0.0021	
V_{min}	0.821	0.906	0.946	0.951		

TABLE II: **Leggett models: critical values and experimental data.** This table shows the critical values of δ_N required to rule out each of the four Leggett-type models discussed in the text. Also shown are measured values for δ_N^1 and δ_N^2 , where the superscript refers to measurements in the $|+\rangle - |L\rangle$ plane, and the $|+\rangle - |H\rangle$ plane of the Bloch sphere, respectively. Bold values have $\delta_N^1 < \delta_N^{\text{crit}}$ and, if required $\delta_N^2 < \delta_N^{\text{crit}}$, i.e. they are ruled out by the data for that N . Note that the measurement in the second, orthogonal plane was only done for $N = 6$. This value is relevant for ruling out the second and fourth cases. In the last row of the table, we note the minimum visibility required to rule out each of the four models.

In order to make $\max_{\alpha} |\alpha \cdot \mathbf{z}|$ as small as possible, i.e. find δ_N^{crit1} , we require the vectors \mathbf{z} to be as far as possible from any of the possible α vectors. If the fixed vector \mathbf{z} is in the plane containing the measurements, this condition leads to $\max_{\alpha} |\alpha \cdot \mathbf{z}| = \cos \frac{\pi}{2N}$ (i.e. \mathbf{z} is positioned exactly in between two settings for α). Hence, this specific version of the Leggett model is falsified if the measured $\delta_N < \delta_N^{\text{crit1}} = \frac{1}{2} \cos \frac{\pi}{2N}$. As shown in Table II, this is the case for all values of N assessed.

According to quantum theory, appropriately chosen measurements on a maximally entangled state lead to correlations for which $\delta_N = \frac{N}{2}(1 - \cos \frac{\pi}{2N})$. However, no experimental realization can be noise-free, and this affects the minimum δ_N attainable (see [16, 31]). One way to characterize the imperfection in the experiment is via the visibility. In an experiment with visibility V , we instead obtain $\delta_N = \frac{N}{2}(1 - V \cos \frac{\pi}{2N})$, which for fixed V has a minimum at finite N . In the case of this model, the minimum visibility required to falsify it is 0.821 (with such a visibility the model could be ruled out with $N = 3$).

Second case: We now suppose \mathbf{z} is a fixed vector, not confined to the plane. Then our basic measurements cannot strictly *rule out* this model: in principle, \mathbf{z} could be close to orthogonal to the plane containing the measurement vectors. (We remark that if \mathbf{z} is completely orthogonal to this plane, then it would not be useful for making predictions.) However, in order to rectify this we can include a second set of measurements in the set of random choices. This set should be identical to the first apart from being contained in an orthogonal plane. We denote the sets \mathcal{A}_1 and \mathcal{A}_2 and we separately measure the δ_N values for each plane, generating values denoted δ_N^1 and δ_N^2 . Analogously to the first case discussed above, this version of the Leggett model is falsified unless for all $\alpha \in \mathcal{A}_1 \cup \mathcal{A}_2$, $|\alpha \cdot \mathbf{z}|/2 \leq \min(\delta_N^1, \delta_N^2)$. In order to make $\max_{\alpha} |\alpha \cdot \mathbf{z}|$ as small as possible, we require the vectors \mathbf{z} to be as far as possible from any of the possible α vectors. Consider now the four vectors $(0, \sin \phi, \cos \phi)$, $(0, -\sin \phi, \cos \phi)$, $(\cos \phi, \sin \phi, 0)$ and $(\cos \phi, -\sin \phi, 0)$ for $\phi \leq \frac{\pi}{4}$ (these represent two neighbouring pairs of measurement vectors (one in each plane), where we have chosen the coordinates such that they are symmetric). The vector equidistant from these (in their convex hull) is $(\frac{1}{\sqrt{2}}, 0, \frac{1}{\sqrt{2}})$. It is then not possible that for all $\alpha \in \mathcal{A}_1 \cup \mathcal{A}_2$, $|\alpha \cdot \mathbf{z}|/2 \leq \min(\delta_N^1, \delta_N^2)$ provided $\max(\delta_N^1, \delta_N^2) < \delta_N^{\text{crit2}} = \frac{1}{2\sqrt{2}} \cos \frac{\pi}{2N}$. As shown in Table II, our experiment, which includes a measurement of δ_6 in an orthogonal plane, also rules out this version of the Leggett model. (The minimum visibility required to rule out this model is 0.906, which could do so using $N = 4$.)

Third case: We consider a slightly modified model in which \mathbf{z} is distributed uniformly over the Bloch sphere. This model is arguably more natural since it is somewhat conspiratorial for \mathbf{z} to always take a particular orientation with respect to the measurements we perform (particularly if that measurement is chosen freely), and is the one referred to in the main text. In this case, defining θ as the angle between α and \mathbf{z} , we compute the left hand side of (17) as

$$\langle D(P_{X|\alpha z}, P_{\bar{X}}) \rangle_{\mathbf{z}} = \int_{\theta=0}^{\pi} d\theta \frac{|\cos \theta| \sin \theta}{4} = \frac{1}{4}.$$

This model is hence excluded if one finds $\delta_N < \delta_N^{\text{crit3}} = \frac{1}{4}$ (measurements are needed only in one plane). As shown in Table II, this is the case for $N \geq 3$. (The minimum visibility required to rule out this model is 0.946, which could do so for $N = 5$.)

Fourth case: Here we return to our measurements in two orthogonal planes and ask whether our data is sufficient to falsify the model for any distribution over \mathbf{z} . (We can think of this in terms of an adversarial picture. Suppose the

set of possible measurement choices is known to an adversary, who can pick the vector \mathbf{z} according to any distribution he likes. The aim is to show that our measurement results are not consistent with any such adversary.) For this model to be correct we need

$$\frac{\langle |\alpha \cdot \mathbf{z}| \rangle_{\mathbf{z}}}{2} \leq \delta_N^1 \text{ for all } \alpha \in \mathcal{A}_1$$

$$\frac{\langle |\alpha \cdot \mathbf{z}| \rangle_{\mathbf{z}}}{2} \leq \delta_N^2 \text{ for all } \alpha \in \mathcal{A}_2.$$

Again we can parameterize in terms of the four vectors introduced previously. When minimizing with respect to these four, we should take $P_{\mathbf{Z}}$ to have support only on the set $(\sin \theta, 0, \cos \theta)$ (going off this line increases the inner product with measurement vectors in both sets). We thus have

$$\langle |\alpha \cdot \mathbf{z}| \rangle_{\mathbf{z}} = \begin{cases} \int_{\theta} d\theta \rho(\theta) \cos \theta \cos \frac{\pi}{2N} & \text{for all } \alpha \in \mathcal{A}_1 \\ \int_{\theta} d\theta \rho(\theta) \sin \theta \cos \frac{\pi}{2N} & \text{for all } \alpha \in \mathcal{A}_2 \end{cases}$$

where $\rho(\theta)$ is the probability density over θ .

In other words, non-zero $\rho(\theta)$ gives contribution $\cos \theta \cos \frac{\pi}{2N}$ to the first integral, and $\sin \theta \cos \frac{\pi}{2N}$ to the second. In order that both integrals are equal, we should take $\rho(\theta)$ to be symmetric about $\theta = \frac{\pi}{8}$. For functions with this symmetry, non-zero $\rho(\theta)$ gives contribution $(\sin \theta + \cos \theta) \cos \frac{\pi}{2N}$ to both integrals. The minimum of this over $0 \leq \theta \leq \frac{\pi}{8}$ is $\cos \frac{\pi}{2N}$, which occurs for $\theta = 0$. It follows that the most experimentally challenging distribution to rule out is $\rho(\theta) = \frac{1}{2}(\delta_{\theta,0} + \delta_{\theta,\frac{\pi}{4}})$, where $\delta_{x,y}$ is the Kronecker delta (this being the distribution that requires the lowest measured δ_N to eliminate). For this distribution, we have $\max_{\alpha} \langle |\alpha \cdot \mathbf{z}| \rangle_{\mathbf{z}} / 2 = \frac{1}{4} \cos \frac{\pi}{2N}$, so this model is ruled out for $\max(\delta_N^1, \delta_N^2) < \delta_N^{\text{crit}4} = \frac{1}{4} \cos \frac{\pi}{2N}$. Again, as detailed in Table II, our experimental data is sufficient to do so. (The lowest visibility that could rule out this case is 0.951, which would do so for $N = 5$).

Comment on minimum visibilities required to rule out Leggett models

Here we briefly compare the visibilities required to rule out Leggett models using our approach with those needed in previously considered Leggett inequalities. We remind the reader that the technique used in the present work generates conclusions that apply to arbitrary theories and were not developed with Leggett's model in mind. Nevertheless, use of this new approach to rule out Leggett models requires comparable visibilities to those of previously discussed inequalities. More specifically, the claimed minimum visibilities are 0.974 in Gröblacher *et al.* [12] and 0.943 for the alternative inequality of Branciard *et al.* [13, 15], which is only slightly below the value we require to rule out all of the four models above.

We note that the visibility for measurements in the plane used in the main text was 0.967 ± 0.007 , while the visibility in the orthogonal plane (measured for the purposes of ruling out the second and fourth cases) was 0.977 ± 0.009 .

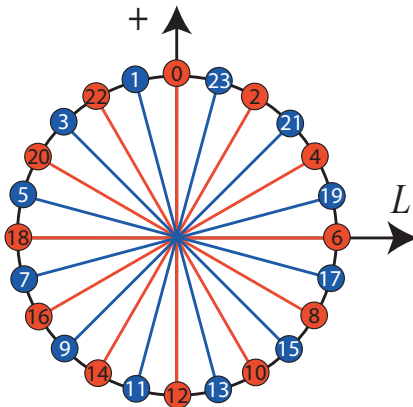


FIG. 4: **Measurement settings for $N = 6$.** All settings are in the $|+\rangle\text{-}|L\rangle$ plane in the Bloch sphere. Alice's settings are indicated in red and Bob's in blue.

Density Matrix and Raw Data

The experimental settings as well as the associated measurement results that allow reconstruction of the density matrix are given in Table III. The most likely density matrix is detailed in Table IV. Note that this density matrix is not used for the calculation of experimental values for δ_N , I_N or ν_N , but is included to characterize our source. The measurements settings used to experimentally determine δ_6 are depicted in Figure 4, and Table V lists the results used to calculate δ_6 from the bi-partite correlation I_6 and the bias ν_6 .

Setting		HWP_A	QWP_A	HWP_B	QWP_B	R_C	ΔR_C
a	b	($^\circ$)	($^\circ$)	($^\circ$)	($^\circ$)	(cps)	(cps)
$ H\rangle$	$ H\rangle$	0	0	0	0	240.0	2.8
$ H\rangle$	$ V\rangle$	0	0	45	0	1.8	0.2
$ H\rangle$	$ +\rangle$	0	0	22.5	45	118.4	2.0
$ H\rangle$	$ -\rangle$	0	0	-22.5	45	125.3	2.0
$ H\rangle$	$ R\rangle$	0	0	0	45	118.7	2.0
$ H\rangle$	$ L\rangle$	0	0	0	-45	130.6	2.0
$ V\rangle$	$ H\rangle$	45	0	0	0	2.0	0.3
$ V\rangle$	$ V\rangle$	45	0	45	0	230.6	2.8
$ V\rangle$	$ +\rangle$	45	0	22.5	45	119.1	2.0
$ V\rangle$	$ -\rangle$	45	0	-22.5	45	118.5	2.0
$ V\rangle$	$ R\rangle$	45	0	0	45	123.8	2.0
$ V\rangle$	$ L\rangle$	45	0	0	-45	112.4	1.9
$ +\rangle$	$ H\rangle$	22.5	45	0	0	115.7	2.0
$ +\rangle$	$ V\rangle$	22.5	45	45	0	122.0	2.0
$ +\rangle$	$ +\rangle$	22.5	45	22.5	45	245.8	2.9
$ +\rangle$	$ -\rangle$	22.5	45	-22.5	45	3.6	0.3
$ +\rangle$	$ R\rangle$	22.5	45	0	45	118.8	2.0
$ +\rangle$	$ L\rangle$	22.5	45	0	-45	111.3	1.9
$ -\rangle$	$ H\rangle$	-22.5	45	0	0	124.2	2.0
$ -\rangle$	$ V\rangle$	-22.5	45	45	0	116.6	2.0
$ -\rangle$	$ +\rangle$	-22.5	45	22.5	45	3.7	0.4
$ -\rangle$	$ -\rangle$	-22.5	45	-22.5	45	241.1	2.8
$ -\rangle$	$ R\rangle$	-22.5	45	0	45	124.5	2.0
$ -\rangle$	$ L\rangle$	-22.5	45	0	-45	138.5	2.1
$ R\rangle$	$ H\rangle$	0	45	0	0	112.7	1.9
$ R\rangle$	$ V\rangle$	0	45	45	0	124.5	2.0
$ R\rangle$	$ +\rangle$	0	45	22.5	45	119.2	2.0
$ R\rangle$	$ -\rangle$	0	45	-22.5	45	121.7	2.0
$ R\rangle$	$ R\rangle$	0	45	0	45	2.9	0.3
$ R\rangle$	$ L\rangle$	0	45	0	-45	239.3	2.8
$ L\rangle$	$ H\rangle$	0	-45	0	0	128.8	2.1
$ L\rangle$	$ V\rangle$	0	-45	45	0	109.0	1.9
$ L\rangle$	$ +\rangle$	0	-45	22.5	45	115.8	2.0
$ L\rangle$	$ -\rangle$	0	-45	-22.5	45	124.6	2.0
$ L\rangle$	$ R\rangle$	0	-45	0	45	230.8	2.8
$ L\rangle$	$ L\rangle$	0	-45	0	-45	4.0	0.4

TABLE III: **Tomographic Data.** This table shows raw data collected to find the density matrix shown in Table IV. The coincidence rates between the Si avalanche photodiode (APD) and the triggered 1550 nm InGaAs APD (R_C) for each set of photon analyzer settings are given in average counts per second (cps), as are their one standard deviation uncertainties (ΔR_C). Settings a and b were implemented using one quarter wave plate followed by one half wave plate in each analyzer. These waveplates were set at angles HWP_A , QWP_A , HWP_A , and QWP_A . Data collection time for each point was 30 seconds.

(a) ρ_{Re}					(b) ρ_{Im}				
	$\langle HH $	$\langle HV $	$\langle VH $	$\langle VV $		$\langle HH $	$\langle HV $	$\langle VH $	$\langle VV $
$ HH\rangle$	0.5038	-0.0052	-0.0092	0.4851	$ HH\rangle$	0.0000	0.0155	0.0138	-0.0140
$ HV\rangle$	-0.0052	0.0040	0.0001	-0.0011	$ HV\rangle$	-0.0155	0.0000	0.0017	-0.0156
$ VH\rangle$	-0.0092	0.0001	0.0043	-0.0044	$ VH\rangle$	-0.0138	-0.0017	0.0000	-0.0113
$ VV\rangle$	0.4851	-0.0011	-0.0044	0.4879	$ VV\rangle$	0.0140	0.0156	0.0113	0.0000

TABLE IV: **Density matrix.** The real and imaginary parts of the density matrix generated by maximum likelihood quantum state tomography.

Setting	HWP_A	HWP_B	R_{Si}	R_C	$1 - P(m, n)$	$P(m, n)$	$\Delta P(m, n)$	ν	$\Delta\nu$
m	n	($^\circ$)	($^\circ$)	(cps)	(cps)				
0	11	0	-41.25	18692	6.7				
0	23	0	-86.25	18597	264.9				
12	23	-45	-86.25	19017	7.5	0.0259	0.9741	0.0011	0.0047 0.0003
12	11	-45	-41.25	18976	270.6				
0	1	0	-3.75	18552	267.3				
0	13	0	-48.75	18588	9.2				
12	13	-45	-48.75	18919	263.0	0.9657	0.0343	0.0012	0.0045 0.0003
12	1	-45	-3.75	18900	9.6				
2	1	-7.5	-3.75	18571	267.8				
2	13	-7.5	-48.75	18632	7.6				
14	13	-52.5	-48.75	18772	263.3	0.9697	0.0303	0.0012	0.0039 0.0003
14	1	-52.5	-3.75	19018	9.0				
2	3	-7.5	-11.25	18528	266.8				
2	15	-7.5	-56.25	18746	8.5				
14	15	-52.5	-56.25	18910	268.4	0.9665	0.0335	0.0012	0.0042 0.0003
14	3	-52.5	-11.25	18990	10.1				
4	3	-15	-11.25	18712	271.2				
4	15	-15	-56.25	18604	7.9				
16	15	-60	-56.25	18430	263.6	0.9720	0.0280	0.0011	0.0029 0.0003
16	3	-60	-11.25	18449	7.6				
4	5	-15	-18.75	18058	262.4				
4	17	-15	-63.75	17979	7.8				
16	17	-60	-63.75	18147	254.3	0.9671	0.0329	0.0012	0.0022 0.0003
16	5	-60	-18.75	18201	9.8				
6	5	-22.5	-18.75	18034	262.0				
6	17	-22.5	-63.75	18129	7.8				
18	17	-67.5	-63.75	18045	261.9	0.9716	0.0284	0.0011	0.0003 0.0003
18	5	-67.5	-18.75	18166	7.5				
6	7	-22.5	-26.25	18044	259.2				
6	19	-22.5	-71.25	18499	8.5				
18	19	-67.5	-71.25	18438	257.9	0.9634	0.0366	0.0013	0.0017 0.0003
18	7	-67.5	-26.25	18360	11.1				
8	7	-30	-26.25	18354	261.9				
8	19	-30	-71.25	18386	7.3				
20	19	-75	-71.25	18317	262.8	0.9735	0.0265	0.0011	0.0002 0.0003
20	7	-75	-26.25	18403	7.0				
8	9	-30	-33.75	18305	261.7				
8	21	-30	-78.75	18254	8.5				
20	21	-75	-78.75	18066	256.7	0.9659	0.0341	0.0012	0.0020 0.0003
20	9	-75	-33.75	18200	9.8				
10	9	-37.5	-33.75	18042	260.4				
10	21	-37.5	-78.75	18102	7.3				
22	21	-82.5	-78.75	18100	257.1	0.9696	0.0304	0.0012	0.0002 0.0003
22	9	-82.5	-33.75	18073	9.0				
10	11	-37.5	-41.25	17979	256.3				
10	23	-37.5	-86.25	17958	9.6				
22	23	-82.5	-86.25	17857	256.3	0.9615	0.0385	0.0013	0.0005 0.0003
22	11	-82.5	-41.25	18014	10.9				

TABLE V: **Raw Data used to calculate δ_6^1 .** This table shows raw data collected to find $\delta_6^1 = 0.1942 \pm 0.0021$. HWP_A and HWP_B are the half wave-plate settings that, together with quarter waveplate settings of -45° on side A and $+45^\circ$ on side B, realize the measurements corresponding to m and n as shown in Figure 4. The free running Silicon APD rates (R_{Si}) and the coincidence rates between the Si APD and the triggered 1550 nm InGaAs APD (R_C) are both given in average counts per second. $P(m, n)$ is the probability of correlated outcomes and ν is the bias for individual measurements as detailed above. Data collection time for each point was 40 seconds. Uncertainties are one standard deviation.